

Initial Integration of Noise Prediction Tools for Acoustic Scattering Effects

Douglas M. Nark*, Casey L. Burley†, Ana Tinetti‡, and John W. Rawls, Jr.§
NASA Langley Research Center, Hampton, VA 23681-2199

This effort provides an initial glimpse at NASA capabilities available in predicting the scattering of fan noise from a non-conventional aircraft configuration. The Aircraft NOise Prediction Program, Fast Scattering Code, and the Rotorcraft Noise Model were coupled to provide increased fidelity models of scattering effects on engine fan noise sources. The integration of these codes led to the identification of several key issues entailed in applying such multi-fidelity approaches. In particular, for prediction at noise certification points, the inclusion of distributed sources leads to complications with the source semi-sphere approach. Computational resource requirements limit the use of the higher fidelity scattering code to predict radiated sound pressure levels for full scale configurations at relevant frequencies. And, the ability to more accurately represent complex shielding surfaces in current lower fidelity models is necessary for general application to scattering predictions. This initial step in determining the potential benefits/costs of these new methods over the existing capabilities illustrates a number of the issues that must be addressed in the development of next generation aircraft system noise prediction tools.

Nomenclature

A	attenuation due to shielding, dB
c_0	speed of sound, (m/s)
f	frequency, Hz
FPA	Flight Path Angle, deg (Figure 6)
N	Fresnel number
PNLT	Tone corrected Perceived Noise Level, dB
$S(f, \theta, \phi)$	ANOPP suppression function
SPL	Sound Pressure Level, dB
x	direction of flight (positive x direction)
Symbols:	
ϕ	azimuthal angle, deg
θ	polar angle, deg

I. Introduction

Aircraft system noise prediction capabilities are necessary to estimate the community noise impact of future aircraft, as well as provide noise impact estimates of changes in propulsion systems, airframes, configurations, and flight operations of current aircraft. Aircraft system noise is the cumulative sum of noise generated by various components of the aircraft propulsion system, as well as various components of the airframe and their interaction effects. Predicting noise on the ground from an aircraft flyover requires estimating the noise generated by the many contributing

*Research Scientist, Structural Acoustics Branch, Research & Technology Directorate. Member AIAA.

†Senior Research Scientist, Aeroacoustics Branch, Research & Technology Directorate. Member AIAA.

‡Senior Principal Software Engineer, Mark H. Dunn Inc. Senior Member AIAA.

§Senior Engineer, Lockheed Martin Space Operations, Langley Program Office.

sources during the flyover as flight conditions change, summing these sources as a function of time, and propagating the resultant combined sources through the atmosphere to the observer locations. NASA introduced the Aircraft NOise Prediction Program about 30 years ago to provide such a capability for predicting the noise from aircraft in flight. NASA has continued to improve these prediction capabilities through validation and advanced modeling developments. The ANOPP system is used by both government agencies and the aircraft industry to assess existing aircraft, as well as evaluate the noise reduction potential of new technologies. This requires that the prediction models of ANOPP be computationally efficient, yet of sufficiently high fidelity to capture the effects on noise of design and/or operational changes. Hence, ANOPP relies primarily on semi-empirical methods for predicting the various aircraft noise sources. Today, there is a need to include prediction capabilities that more accurately capture the noise source generation, as well as the effects of acoustic scattering and atmospheric propagation. These capabilities are critical for the use of predictions in design and evaluation of not only conventional, but even more so of non-conventional configurations and flight procedures. Thus, there is a need to extend many of the semi-empirical approaches currently in use.

This effort examines NASA aircraft noise prediction capabilities for determining noise from a non-conventional aircraft with a hybrid wing. Specifically, the Silent Aircraft eXperimental (SAX 40) aircraft configuration¹ with podded engines was considered. This configuration has many of the same noise sources found for conventional aircraft (see Figure 1), such as those from the engine and airframe, but the effects of engine noise scattering from the airframe are significantly different. The Aircraft NOise Prediction Program (ANOPP),² Fast Scattering Code (FSC),³ and the Rotorcraft Noise Model (RNM)⁴ were coupled to provide increased fidelity models of scattering effects on engine fan noise sources. The study is intended to give a view of the issues entailed in coupling the codes of varied disciplines and fidelity, as well as provide an initial glimpse at NASA capabilities available in predicting the scattering of fan noise. It is an initial step in determining the potential benefits/costs of these new methods over the existing capabilities of ANOPP. The knowledge and understanding gained from this will provide a basis for the development of next generation aircraft system noise prediction capabilities.

II. System Noise Prediction Approach

Aircraft system noise consists of components associated with the propulsion system (such as jet, fan, compressor, combustor, propeller, and turbine noise), components associated with the airframe (such as landing gear, flap, slat, and trailing edge noise), and those associated with installation effects due to configuration (engine sources shielded by the fuselage). The importance of each source may vary with aircraft configuration and operating condition.

Prediction capabilities for aircraft system noise are on a hierarchy that trades fidelity versus range of applicability. On one end of the hierarchy are the acoustic research codes based on first principles. These codes require high fidelity aerodynamic and geometric inputs. They are used to determine the specific physics responsible for the noise generation. They tend to be somewhat limited in range of applicability and validity in that they address narrowly-focused acoustic phenomena at a component or flow physics level. The results are often not readily or easily extended to community noise metrics. These research codes generally are non-commercial (*i.e.*, of limited availability), require expert users, and are computationally intensive.

On the opposite end of this hierarchy are prediction capabilities that are of low fidelity but have a large range of application. These codes may predict multiple-event noise metrics at the airport level for an entire fleet of aircraft and are typically widely-available, empirically based, and quick to execute. However, they are often validated only for current configurations, where the noise characteristics are assumed to be known.

NASA's aircraft system noise prediction tool, Aircraft NOise Prediction Program (ANOPP),² lies somewhere between the low and high fidelity prediction methods. NASA introduced ANOPP in the early 1970s for predicting the noise from aircraft in flight and has continued to improve, extend and add new prediction capabilities through validation and advanced modeling developments. ANOPP has primarily been developed and validated for conventional aircraft configurations where the airframe and engine noise sources are analyzed in isolation. The modeling of installation effects due to configuration is very limited. The methods are predominately empirical to semi-empirical and hence are most applicable to aircraft configurations on which they were based. To extend these capabilities to non-conventional aircraft, a strategy is being considered to replace low fidelity empirical methods with higher fidelity analyses. Ideally, a noise prediction system would be comprised of the highest fidelity tools possible. However, this is currently not viable due to computational expense (*i.e.*, CPU time, memory requirements). Intermediate steps to ensure that the benefits of higher fidelity methods outweigh their relative cost must be determined. Initial utilization of these methods in current noise prediction systems will be a first step toward this goal. Figure 2 schematically shows how a higher fidelity analysis may be coupled with ANOPP. In this example, the effect of the airframe on a fan source

noise in terms of a noise suppression factor is computed external to ANOPP using the high fidelity analysis FSC. The FSC computations for the scattered noise field are modified for direct input to ANOPP as a fan noise suppression factor defined on a semi-sphere surrounding the vehicle.

A. ANOPP

A schematic of the ANOPP system is shown in Figure 3. ANOPP consists of a set of functional modules that compute atmospheric properties, aircraft flight path, source-to-observer geometry, source noise of the aircraft components (propulsion systems and airframe), propagation of the source noise to ground observers, and community noise metrics. Not shown, but an important part of the capability is the ANOPP executive. It controls the execution of modules, provides data management for the functional modules and provides error handling and exit procedures to the host computer.

There are multiple methods in ANOPP to model the various noise sources. The particular source noise modules used in the study are identified in Table 1. The Fink method,^{5,6} was chosen to predict the wing and winglet trailing edge noise. It is noted that none of the ANOPP methods include a capability to predict noise from a deployed eivon and hence this source was modeled using the Fink method as a trailing edge source in the undeployed position. The Guo method⁷ was chosen to predict the landing gear noise since it has been validated with full scale gear of similar size. The engine sources considered in this study are the jet, fan (aft and inlet), and combustor components. The Stone II model is the most current method within ANOPP for predicting jet noise. This method unifies the previous Stone methods⁸ into one capability applicable to engines with bypass ratios ranging from 0 to about 14. The fan noise is predicted using the Heidmann fan method for large fans^{9,10} and the combustor noise is predicted using the GECOR module.^{11,12}

Noise Source	ANOPP Module	Theoretical Basis
Airframe (wing/ body trailing edge, winglets)	FNKAFM	Fink ^{5,6}
Landing gear (nose and main)	BAF	Guo ⁷
Jet	ST2JET	Stone ⁸
Fan	HDFAN	Heidmann, ⁹ Kontos ¹⁰
Combustor	GECOR	Matta ^{11,12}

Table 1. ANOPP modules used in study

1. Noise shielding

The engines are located on the upper surface of the SAX 40 airframe, thus shielding noise from observers on the ground. For this study the fan inlet and aft fan sources are the only engine sources considered for attenuation due to fuselage scattering. Within ANOPP, the effects of a barrier may be modeled in two ways (1) by adjusting the source directivity or (2) by adjusting the propagated noise at the observer. Adjustment of the source directivity is achieved by applying a suppression table to the predicted source noise. This table is generated by calculating a suppression function for each frequency at every polar, θ , and azimuthal, ϕ , angle on the noise source semi-sphere. The suppression function, S , is the ratio of the shielded to unshielded mean square pressures and is given by

$$S(f, \theta, \phi) = \frac{P_{rms}^2(f, \theta, \phi)_{shielded}}{P_{rms}^2(f, \theta, \phi)_{unshielded}} = 10^{\left(\frac{\Delta dB}{10}\right)} \quad (1)$$

where $\Delta dB = SPL_{shielded} - SPL_{unshielded}$. Thus, $S < 1$ indicates suppression and $S > 1$ indicates amplification. In this paper, the suppression function is determined using the FSC code, further details of which are given in the next section.

In the second approach, the WING module in ANOPP is used to adjust the propagated noise at the observer. The method is based on the work of Maekawa¹³ and Kurze and Anderson,¹⁴ who developed methods for predicting the insertion loss of sharp-edged barriers in terms of a Fresnel number. Beranek¹⁵ modified the Kurze and Anderson formulation to address the transition region between the fully shielded and unshielded zones. Within the WING module, the effect of noise shielding is computed and applied to the propagated source noise for each observer location and each time step. For each time step, it is determined if a direct ray from the source to the observer intersects a barrier (*i.e.*, wing surface). If the ray does not intersect the wing surface, no attenuation is computed or applied. If the ray

intersects the wing surface, then shielding attenuation is computed for each of the 1/3 octave center band frequencies and applied to the received mean-square pressures as follows:

$$P_{rms}^2(f, \theta, \phi)_{\text{shielded}} = P_{rms}^2(f, \theta, \phi)_{\text{unshielded}} - A_{TOT}(f, \theta, \phi) \quad (2)$$

where $P_{rms}^2(f, \theta, \phi)_{\text{unshielded}}$ is the unshielded level at the observer and A_{TOT} is the total attenuation due to shielding from the combined effects of the three diffraction edges (wing trailing, leading and tip edges) summed as mean-square pressures. For each edge the attenuation (A_k) due to shielding is computed as

$$A_k(f) = \begin{cases} 20 \log_{10} \frac{\sqrt{2\pi N}}{\tanh \sqrt{2\pi N}} + 5 & N \geq 0 \\ 20 \log_{10} \frac{\sqrt{2\pi N}}{\tan \sqrt{2\pi N}} + 5 & -0.2 \leq N < 0 \\ 0 & N < -0.2 \end{cases} \quad (3)$$

The Fresnel number N is defined as

$$N = 2f\Delta/c_0 \quad (4)$$

where f represents each 1/3 octave band center frequency and Δ is the difference in source-receiver path length between the direct and diffracted sound fields. The maximum attenuation in ANOPP is limited to 24 dB due to modeling considerations provided in Kurze¹⁴ and Beranek.¹⁵

ANOPP assumes the wing to be planar and only allows 4 points in its definition. The points must be located on the root leading and trailing edges, and the wing tip leading and trailing edges. In addition, the shielding is assumed symmetric with respect to the fuselage centerline and hence need only be defined over half the span. This obviously poses limitations for modeling the airframe of the SAX 40, as shown in Figure 4. The rationale used to define the four wing points, was to include as much of the wing in the lateral direction while closely approximating the fuselage leading, trailing edges. This prevented the prediction of excess shielding of the forward fan noise at ground observers.

B. Fast Scattering Code

FSC^{3,16} predicts the three-dimensional scattered acoustic field produced by the interaction of a known, time-harmonic, incident sound (such as the field produced by spinning mode acoustic pressure waves exiting an engine duct) with structures of arbitrary geometry (wings, nacelles, fuselages, pylons). It is assumed that the scattering bodies and the co-moving acoustic sources are immersed in a potential flow field. The FSC has been developed for use as an aeroacoustic analysis tool for assessing the effects on noise radiation and scattering caused by changes in configuration (geometry, component placement) and operating conditions (background flow, excitation frequency). The method is based on the equations of linearized acoustics and employs the Equivalent Source Method (ESM) to solve an exterior Helmholtz equation boundary value problem (BVP).

The central idea of the ESM is to approximate the solution to the BVP with a superposition of simple sources (point monopoles, dipoles, or any multipole combination) located inside the scatterers and determine the strengths of these sources so that an impedance type boundary condition is satisfied, in the least squares sense, on the scattering surfaces. The FSC solution strategy has four steps: 1) discretization of the scattering surfaces according to excitation frequency, 2) generation and placement of equivalent sources, 3) solution of the complex equivalent source matrix, and 4) computation of the acoustic field at the observer points. The code features fast numerical calculations that can be performed on personal computers or workstations for moderate excitation frequencies. The FSC has been applied to various acoustic scattering simulations involving full-scale commercial transport components.¹⁷ Work is ongoing to produce an updated version of the FSC that utilizes Fast Multipole Methods to increase the frequency limits.¹⁸ The updated version was not available for this investigation and therefore predictions for this paper are limited to frequencies less than 400 Hz full scale.

As part of this assessment exercise, the FSC was used to generate input data for both ANOPP and RNM. In connection with ANOPP, FSC was used to generate a suppression table, thereby bypassing the WING module and applying shielding effects, in terms of a suppression function, directly on the source noise semi-sphere. Additionally, FSC was used to generate an input source semi-sphere for RNM, which was subsequently used to produce noise footprints. These footprints illustrate the noise scattering effects of both nacelles and full fuselage. The details of both procedures are presented in section C, however a brief description of RNM, as well as the example problem considered, are in order before proceeding.

C. Rotorcraft Noise Model

RNM⁴ is a simulation program that models sound propagation through the atmosphere, computing a variety of noise metrics at receiver locations on flat ground or varying terrain. It was initially created for the purpose of (1) assessing low noise terminal area aircraft operating procedures, and (2) providing an improved aircraft community noise impact modeling capability. Development of RNM began in the mid-1990s and continues with on-going improvements. The major computational elements of RNM are the sound propagation module and the input/output modules. As input, RNM requires source noise semi-spheres, aircraft flight track, flight profile orientation and operating state. Vehicle operations are quantified along a set of user-defined, vectored flight tracks. The vehicle flight is simulated in a time-based domain along flight tracks and the sound analytically propagated through the atmosphere to the user-specified receiver locations. RNM currently accounts for spherical spreading, atmospheric absorption, ground reflection and attenuation, wind and temperature gradients, and terrain effects, Doppler shifts, and the difference in phase between the direct and reflected rays.

The input source noise semi-spheres required by RNM represent the noise source(s) field, such as that surrounding an aircraft for a given steady state operating conditions. These may be obtained through vehicle flight testing over a range of conditions,⁴ theoretical predictions, wind tunnel experiments, or a combination of the three. When used in RNM, the source noise semi-sphere translates and rotates with the vehicle trajectory and orientation. Each sound semi-sphere contains acoustic information for a single aircraft flight condition and the appropriate independent variables such as airspeed and engine power setting.

III. Results and Discussion

A. Vehicle Description

The key vehicle parameters for the SAX 40 configuration are given in Table 2 and represent a consolidation of parameters available in the following references:^{1,19} Some parameter values were found to be inconsistent in the references; the authors at MIT were consulted²⁰ for a resolution. The parameters in Table 2 were used as input to ANOPP noise modules.

The engine details used for the SAX 40 design are proprietary. Fortunately, NASA has the capability to compute needed propulsion data using a thermodynamic cycle and aeromechanical engine simulation program known as the Numerical Propulsion System Simulator (NPSS).²¹ The proposed engine thrust for the SAX-40 was provided by MIT.²⁰ Based on a thrust-to-weight ratio for similar sized aircraft as the SAX 40, the CFM56-7B engine was found to most closely provide the appropriate thrust requirements. A generic engine modeled after the design of a CFM56-7B was analytically modeled within NPSS using data available from several reliable public-domain information sources, such as FAA type certification data sheets, manufacturer-provided airport planning documents, library technical reports, Jane's Aero Engines, and manufacturer's websites. The NPSS simulation was easily configured to determine the pressures, temperatures, rotational speeds, and flow areas for each flow station within the engine for inclusion in the ANOPP input file. Within ANOPP, the engine parameters were adjusted based on area scaling to match the engine thrust provided by MIT.²⁰

	Aircraft Parameter Value (nominal)
Wing Area	918 m ² (9880 ft ²)
Wing span (not including winglet)	63 m (207 ft)
Centerbody Area	639 m ² (6876 ft ²)
Centerbody Span	26.5 m (84 ft)
Winglet Area	33 m ² (109 ft ²)
Winglet Span	4.3 m (14 ft)
MTOW	150,845 kg (332, 560 lbs)
Nose and Main Gear Tire Diameter	1.27 m (4.17 ft)
# of Main Gears	2
# of Tires per Main Gear	4

Table 2. Concept SAX 40 geometric parameters^{19,20,22}

B. Flight Procedure

The trajectory is important for accurate prediction of any time-dependent aircraft noise metric. The noise propagated through the atmosphere to the ground is dependent on the location, direction, orientation, airspeed, engine throttle setting, and operational configuration of the aircraft. These are all functions of time aircraft position. For an existing aircraft, these data may be obtained from measurement, where an aircraft trajectory is tracked using radar equipment, optical systems or other means. However for a conceptual aircraft, such as the SAX 40, these are obtained from trajectory simulations. Analytical trajectory simulations can be complex solutions of equations of motion, using aircraft aerodynamic, thrust performance, stability and control moment, weight, and atmospheric data. Many times the aircraft aerodynamics, in the form of so-called “drag polars,” and stability and control data are needed, but are often proprietary. The trajectories for the SAX 40 were provided by MIT²⁰ for a certification procedure described according to FAR 36. Profiles for altitude, net thrust, and flight path angle (FPA) as a function of distance from brake release are shown in Figure 6 for the takeoff procedure (includes the initial climb and the cutback segment). Due to the predicted low speed performance characteristics of the SAX 40, the initial climb segment requires an engine throttle setting of only 68%. The cutback segment begins when the aircraft is approximately 5200 m (17080 ft) from brake release with the engine throttle reduced to 36%. The approach profile is not shown, but was performed with a -3 degree flight path angle, a nominal vehicle angle-of-attack of 12°, engine throttle setting of 7.5%, and a flight velocity of 70 m/s (230 ft/sec).

The noise certification measurement locations for which predictions are presented are shown in Figure 5. The approach measurement location is 2000 m upstream of the runway, which places the vehicle at an altitude of 120m (394 ft). The sideline location is offset from the flight track by 450m (1476 ft) and its streamwise location is determined by the maximum noise level that occurs during the initial climb segment. Nominally this has been found to be approximately 305m (1000ft) altitude. This nominal location is used for the results shown in this paper. The flyover location is defined to be 6500 m (21325 ft) from the start of ground roll as indicated in Figure 5.

C. Prediction Results

In the following sections, predictions obtained using ANOPP with its wing shielding method (WING module) are presented. These preliminary findings are followed by results from coupling FSC with RNM for a level flight profile. Finally, a set of example calculations involving the use of FSC results in ANOPP as an alternative to the WING module are presented. These predictions are compared with the previous ANOPP results (using the WING module) to investigate discrepancies between the two approaches.

ANOPP-WING

Predictions using ANOPP with and without shielding (via the WING module) on the propagated fan noise were are shown in Figures 7 and 8. The total PNLT time histories along with components for airframe and engine noise are presented for the approach and flyover locations. Each figure has the predictions for which the fuselage is not accounted for and ones for which the ANOPP WING shielding module was applied to the fan noise. At the approach location (Figure 7), the inlet fan noise component is seen to dominate the overall total noise levels prior to overhead ($\theta = 90^\circ$) for the unshielded case. When the shielding is applied, both the inlet and to a lesser extent the aft radiated fan noise are significantly reduced prior to overhead, on the order of 10-20 dB. The total noise (sum of all components) is reduced by approximately 7 dB. Other noise sources, such as landing gear (assumed to be similar to complexity of Boeing 777 landing gear), become the major contributors to the overall level once the fan noise has been reduced. At the flyover location (Figure 8) similar trends are seen. The fan inlet source again dominates the overall level prior to overhead. The fuselage shields the inlet fan noise at this location but the aft fan noise is not shielded at all. The accuracy of the predictions can not be fully assessed at this time due to lack of data. However, this represents the current level of prediction capability available with ANOPP.

FSC-RNM

These calculations are the first coupling of FSC output to RNM input. The cases considered are limited. For the FSC predictions, the fan source is taken to be located within the engine nacelle at the fan face and the source parameters are chosen such that the $m=0$ circumferential mode and all associated radial modes are generated. This simplified model is used for a number of reasons. First and foremost, as mentioned previously, information on the actual SAX 40 engine is currently proprietary. Secondly, the focus of this study is to investigate the scattering from the SAX configuration. Several pertinent experimental investigations, with which comparisons may be made, have used point

sources to model the engine noise source.^{23,24} Finally, incorporation of a full fan model within this prediction process would entail the coupling of a fan source code and duct propagation code. The output of which would then be passed onto the FSC for scattering predictions. As an example, the coupling of output from the V072 fan source prediction code²⁵ to the duct propagation and radiation code CDUCT-LaRC²⁶ has been accomplished. However, the capability to properly transfer data to the FSC is not currently in hand. This is left for future investigation. The present use of the simplified fan source model, as well as comparison to the aforementioned experimental work, lead to the use of noise level differences, as opposed to absolute noise levels, in the results to follow.

The computational resources required by the current version of the FSC limits the maximum frequency that may be considered. Predictions were limited to 50, 100, 200, and 400 Hz. The scattered noise field from FSC is reformulated for RNM input as noise levels on a semi-sphere surrounding the vehicle. Points on the semi-sphere are described in terms of a fixed radius and two spherical angles, θ and ϕ , representing the sphere azimuth and elevation angles. The vehicle nose is where θ is 0° and the tail is where θ is 180° , with the port and starboard sides at $\phi = -90^\circ$ and $\phi = 90^\circ$, respectively. For the predictions presented, the source semi-sphere was taken to be 45.72 m (150 ft) in radius and centered on the fan face of the center nacelle. An observer for whom the vehicle is directly overhead would be located at $\theta = 90^\circ$, $\phi = 0^\circ$. It is recognized that for lower frequency noise sources, this semi-sphere may not be in the farfield. In these cases, the directivity patterns would vary with semi-sphere radius due to scattered noise location differences and the summation of coherent sources. However, for certification flight profiles, particularly approach, the size of the source semi-sphere is limited due to the altitudes considered (*i.e.* RNM will not allow the semi-sphere to intersect the ground plane). It is for this reason that the current semi-sphere radius was chosen. This is an issue that needs to be addressed in future work and should be kept in mind when viewing both predicted and experimental results.

Figure 9 presents the steps involved in performing scattering predictions for the full configuration at 200 Hz. The process begins with the prediction of radiated SPL from the single center nacelle. The prediction for the three nacelle configuration is constructed by first calculating source semi-spheres for each individual nacelle separately, taking into account scattering from the other two nacelles. Their relative locations are taken into account due to their position within the source semi-sphere. The three semi-spheres are then summed as incoherent sources (*i.e.*, phase is not taken into account) to obtain the overall SPL directivity shown in Figure 9b. Note that the directivity differs from that obtained for the single center nacelle indicating the effect of the nacelle separation. This differs from the ANOPP approach in which the sources are co-located, the end result being equivalent to summing the center nacelle result three times. Finally, in Figure 9c, the effects of scattering from the full configuration on the SPL directivity pattern are shown. The general shielding effects of the airframe are evident in reduced levels forward and below the aircraft.

The predicted shielding effects may be examined further by considering the difference between the semi-spheres of Figures 9c and 9b. This leads to Δ SPL contours representing the difference in radiated SPL between the shielded and unshielded three nacelle configuration. Positive values indicate amplification, while negative values indicate suppression. In Figure 10 the results for 100 and 200 Hz are shown. The three-dimensional semi-spheres have been replaced by two-dimensional projection contour plots with the nose/tail on the right/left sides and the port/starboard sides on the top and bottom, respectively (*i.e.* the aircraft moves from left to right). The predictions show increased shielding toward the front of the aircraft ($\theta < 90^\circ$). However, some amplification is predicted along diagonal directions aft of the aircraft and at large azimuthal angles and may in part be attributed to interaction with the winglet. The source semi-spheres obtained at the four frequencies were general qualitatively in agreement with measurements presented in aforementioned experimental work.^{23,24}

The source noise semi-spheres were subsequently input to RNM to produce noise footprints for level flight over a flat ground plane using standard atmospheric conditions. A straight and level flight path was assumed at an altitude of 120.1 m (394 ft) and speed of 65.5 m/s (215 ft/s). The footprints showing the difference in SPL between the shielded and unshielded configurations are presented in Figures 11. The vehicle is located at the origin ($x = 0$, $y = 0$) of the plot and is shown to scale in the figures. The main purpose for performing these calculations was to demonstrate the FSC-RNM coupling capability. However, it is worthwhile to note that the footprints show trends that are similar to the corresponding source semi-spheres, as might be expected with uniform conditions (*e.g.* no winds). In particular, the results including the airframe shielding (Figure 11) show a large shadow zone forward of the aircraft with associated increased levels along diagonal directions aft of the aircraft at the lower frequency.

ANOPP-FSC

As in the case of the FSC-RNM coupling, these sample calculations are the first coupling of FSC output to ANOPP input. Here, the FSC computations were used to produce a suppression table (see Equation 1) used within ANOPP as an alternate method to account for the effect of the fuselage on fan noise. The FSC calculations were performed to frequencies up to 400 Hz, due to the previously mentioned computational restrictions. To proceed with the computations,

the suppression function values at frequencies above 400 Hz were set equal to the 400 Hz suppression value. Aside from underestimating the increased suppression that should occur at higher frequencies, this also leads to a constant amplification at some locations that is expected to be diminishing toward suppression. These effects are visible in the results to follow. This is clearly an over-simplified and conservative assumption and is another issue that must be addressed to make the approach viable for future use.

Another point should be mentioned prior to making comparisons between the ANOPP-WING and ANOPP-FSC results. Specifically, there is a difference in the character of the fan sources considered in the two approaches. In the FSC, the fan source to be scattered by the airframe contains the effects of the engine nacelle, as well as the interaction of the three engines (see for example Figure 9). Conversely, ANOPP considers the inlet and aft fan noise as isolated sources, each being located at a single point with its corresponding directivity function applied. Thus, one might generally expect the ANOPP-FSC results to show lower suppression values than the ANOPP-WING predictions due to the presence of the nacelle and multiple engine interaction effects in the fan source.

With the aforementioned issues in mind, PNLT comparisons of the ANOPP-FSC predictions with the ANOPP-WING predictions for fan noise are shown in Figure 12 for the 3 certification locations. The lines labeled “TOTAL” are the total unshielded fan noise levels predicted by ANOPP and the solid triangle symbols on the time axis indicate the times for which the vehicle is at the polar directivity angles of 45°(prior to overhead), 90°(overhead) and 135°(passed overhead). For all three locations, the ANOPP-WING results show much larger noise reduction due to shielding than the ANOPP-FSC results, particularly prior to overhead. At times near overhead, the ANOPP-FSC predicts levels slightly greater than the total unshielded fan noise results. After overhead, all the predictions are nearly identical, indicating that neither fan source (inlet or aft fan noise) is affected by the fuselage.

Contours of Δ EPNL are shown in Figures 13 and 14 for the approach and takeoff flight profiles, respectively. The Δ EPNL is defined as the difference between the baseline contour map (without accounting for shielding) and the EPNL predictions including shielding using either the suppression table from FSC or the ANOPP WING module. This is computed on a dB basis to indicate the noise reduction potential. Negative values indicate a noise reduction due to fuselage scattering/shielding effects. For the approach flight condition (Figure 13), the centerline line values compare favorably. To the sides of the flight path however, the ANOPP-FSC results show no suppression. In fact, although the contour levels are truncated at zero, there are some observer locations where increases of up to one dB were predicted. The increased noise levels for FSC shielding are in part due to the 400 Hz suppression values being used to represent all frequencies up to 10 kHz in ANOPP. On the other extreme, the ANOPP WING module most likely overpredicts the suppression, since it basically models the shielding effect as a barrier. The difference in results from these two methods can clearly be seen in the PNLT presentation of Figure 12. Comparison with measurement is needed to fully assess each of these models. The takeoff profile (Figure 14) includes the sideline and cutback operating conditions. The centerline predictions are in reasonable agreement, particularly near the later portion of the flight profile. However, the ANOPP-FSC again show greatly reduced suppression values to the sides of the flight path. Thus, while comparison of the centerline predictions provide some encouragement, it is clear that the issues of assumed suppression values above 400Hz must be resolved for sideline location predictions in particular.

IV. Concluding Remarks

This work provides a glimpse at NASA capabilities available in predicting the scattering of fan noise from a non-conventional hybrid wing configuration. The FSC-RNM and FSC-ANOPP approaches were considered for the first time. Some of the issues involved in coupling the various acoustic prediction codes to provide an integrated (system level) fan noise prediction are identified. A number of these are summarized as follows:

- The specification of the source semi-sphere radius and frequency limitations were important aspects of the FSC-RNM and FSC-ANOPP approaches. For frequencies at which the source semi-sphere is not in the farfield, the directivity pattern will vary with semi-sphere radius. Testing a series of increasing semi-sphere radii until the directivity patterns converge would appear an appropriate resolution. However, for certification flight profiles, particularly approach, the size of the source semi-sphere is limited due to the altitudes considered (*i.e.* RNM will not allow the semi-sphere to intersect the ground plane).
- Correctly accounting for phase is very important as enhanced methods are utilized in attempting to address distributed, coherent noise sources.
- Work to extend the frequency range for FSC predictions is ongoing and will be necessary to make the FSC-RNM approach viable. Even as this upper limit is increased however, there will be a need to address the remaining suppression values at the highest frequencies for the FSC-ANOPP approach.

- Enhancement of the ANOPP-WING module to incorporate multiple, more complex scattering surfaces is necessary to properly account for non-conventional configurations.
- Data with which to validate SAX 40 noise sources, in particular the shielding effects and improved engine source definition, will be important and critical in pursuing further assessment efforts.

Resolution of these various issues is required in formulating viable approaches to fan noise scattering prediction from conventional and non-conventional configurations. This study provides essential knowledge and some first steps in the development of a next generation aircraft system noise prediction capabilities.

V. Acknowledgments

The authors wish to thank the MIT Gas Turbine Laboratory team, particularly Dr. Zoltan Spakovszky and Mr. Leo Ng for guidance on the SAX-40 geometry and providing the flight operations used in this study. The authors gratefully acknowledge Dr. Jeff Berton for providing NPSS engine simulation data and guidance on engine sizing used for this study. The authors also thank Mr. D. Stuart Pope for assistance with the RNM calculations and Dr. Mark H. Dunn for his expertise and guidance relating to the FSC predictions.

References

- ¹Manneville, A., Pilczner, D., and Spakovszky, Z., "Preliminary Evaluation of Noise Reduction Approaches for Functionally Silent Aircraft," *AIAA Journal*, Vol. 43, No. 3, 2006, pp. 836–840.
- ²Zorunski, W. E., "Aircraft Noise Prediction Program Theoretical Manual," NASA TM 83199, National Aeronautics and Space Administration, 1982.
- ³Tinetti, A. F., Dunn, M. H., and Pope, D. S., "Fast Scattering Code (FSC) User's Manual - Version 2," NASA CR 2006-214510, October 2006.
- ⁴Conner, D. A. and Page, J. A., "A Tool for Low Noise Procedures Design and Community Noise Impact Assessment: The Rotorcraft Noise Model (RNM)," Presented at Heli Japan 2002, Tochigi, Japan, November 2002.
- ⁵Fink, M., "Airframe Noise Prediction Method," FAA-RD 77-29, U.S. Department of Transportation, Federal Aviation Administration, 1977.
- ⁶Fink, M., "Noise Component Method for Airframe Noise," *Journal of Aircraft*, Vol. 16, No. 10, 1979, pp. 659–665.
- ⁷Guo, Y., "Empirical Prediction of Aircraft Landing Gear Noise," NASA CR 213780, National Aeronautics and Space Administration, 2005.
- ⁸Stone, J. R., Krejsa, E. A., and Clark, B. K., "Jet Noise Modeling for Suppressed and Unsuppressed Aircraft in Flight," Contract nas3-00178, task order no. 10, final report, Modern Technologies Corporation, October 2003.
- ⁹Heidmann, M. F., "Interim Prediction Method for Fan and Compressor Source Noise," NASA TM X-71763, 1979.
- ¹⁰Kontos, K., Janardan, B., and Gliebe, P., "Improved NASA-ANOPP Noise Prediction Computer Code for Advanced Subsonic Propulsion Systems Volume I: ANOPP Evaluation and Fan Noise Model Improvement," NASA CR 195480, 1996.
- ¹¹Society of Automotive Engineers, *Gas Turbine Jet Exhaust Noise Prediction*, SAE Aerospace Recommended Practice ARP876, 1994.
- ¹²Emmerling, J. J., Kazin, S. B., and Matta, R. W., "Core Engine Noise Control Program. Volume III, Supplement 1 - Prediction Methods," FAA RD 74-125, 1976.
- ¹³Maekawa, Z., "Noise Reduction By Screens," *Applied Acoustics*, Vol. 1, No. 3, 1983, pp. 157–173.
- ¹⁴Kurze, U. J. and Anderson, G. S., "Sound Attenuation by Barriers," *Applied Acoustics*, Vol. 4, No. 1, 1970, pp. 35–53.
- ¹⁵Beraneck, L. L., *Noise and Vibration Control*, McGraw-Hill Book Company, 1971.
- ¹⁶Dunn, M. H. and Tinetti, A. F., "Aeroacoustic Scattering Via the Equivalent Source Method," AIAA Paper 2004-2937, 2004.
- ¹⁷Tinetti, A. F. and Dunn, M. H., "Aeroacoustic Noise Prediction Using the Fast Scattering Code," AIAA Paper 2005-3061, 2005.
- ¹⁸Dunn, M. H. and Tinetti, A. F., "Application of Fast Multipole Methods to the NASA Fast Scattering Code," AIAA Paper 2008-2875, 2008.
- ¹⁹Hileman, J. I., Reynolds, T. G., de la Rosa Blanca, E., Law, T. R., and Thomas, S., "Development of Approach Procedures for Silent Aircraft," AIAA Paper 2007-451, 2007.
- ²⁰Spakovszky, Z. S. and Ng, L., Personal Communication, March 2008.
- ²¹Lytte, J. K., "The Numerical Propulsion System Simulation: An Overview," NASA TM 209915, National Aeronautics and Space Administration, 2000.
- ²²Crichton, D., de la Rosa Blanco, E., Law, T. R., and Hileman, J. I., "Design and Operation for Ultra Low Noise Take-off," AIAA Paper 2007-456, 2007.
- ²³Reimann, C. A., Tinetti, A. F., and Dunn, M. H., "Noise Prediction Studies for the Blended Wing Body Using the Fast Scattering Code," AIAA Paper 2005-2980, 2005.
- ²⁴Agarwal, A., Dowling, A. P., Shin, H., Graham, W., and Sefi, S., "A Ray Tracing Approach to Calculate Acoustic Shielding by the Silent Aircraft Airframe," AIAA Paper 2006-2618, 2006.
- ²⁵Meyer, H. D. and Envia, E., "Aeroacoustic Analysis of Turbofan Noise Generation," NASA CR 4715, 1996.
- ²⁶Nark, D. M., Farassat, F., Pope, D. S., and Vatsa, V., "The Development of the Ducted Fan Noise Propagation and Radiation Code CDUCT-LaRC," AIAA Paper 2003-3242, 2003.

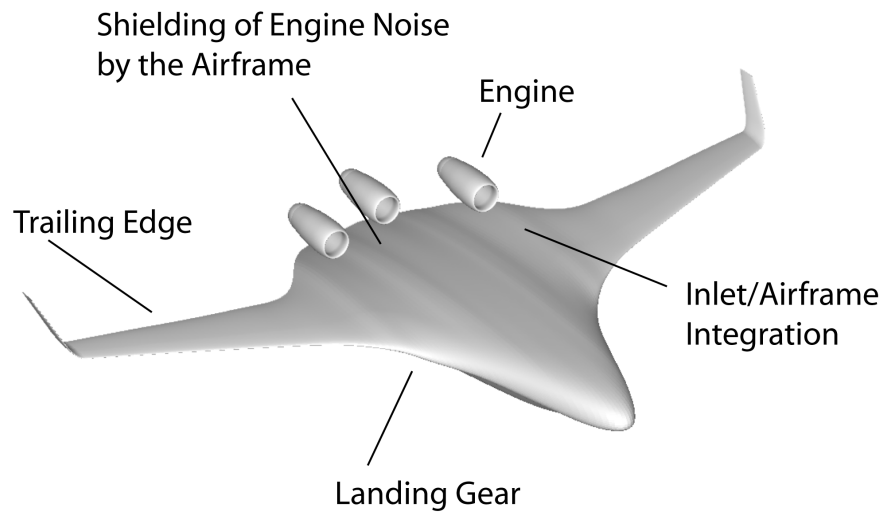


Figure 1. SAX 40 key noise issues

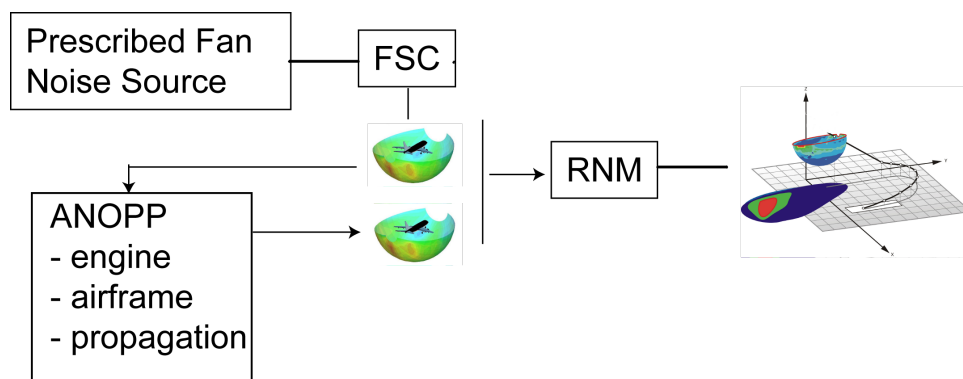


Figure 2. Example work flow involved in coupling variable fidelity analyses.

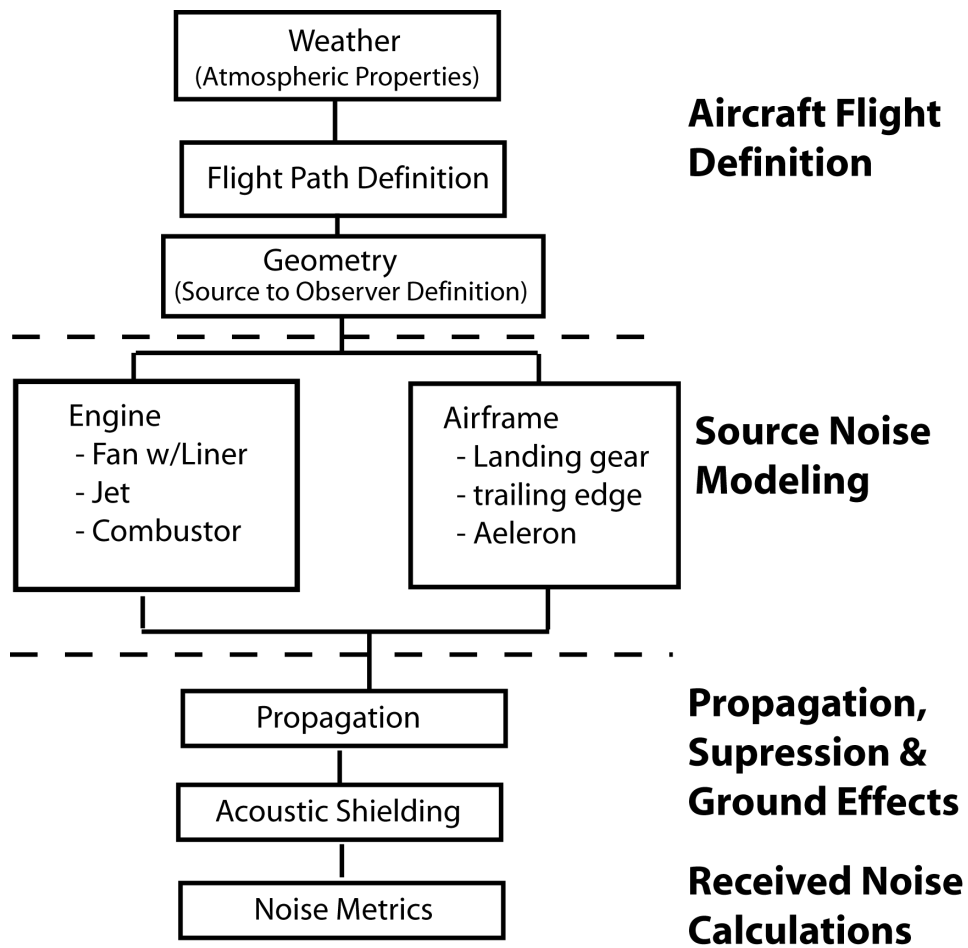


Figure 3. ANOPP work flow diagram

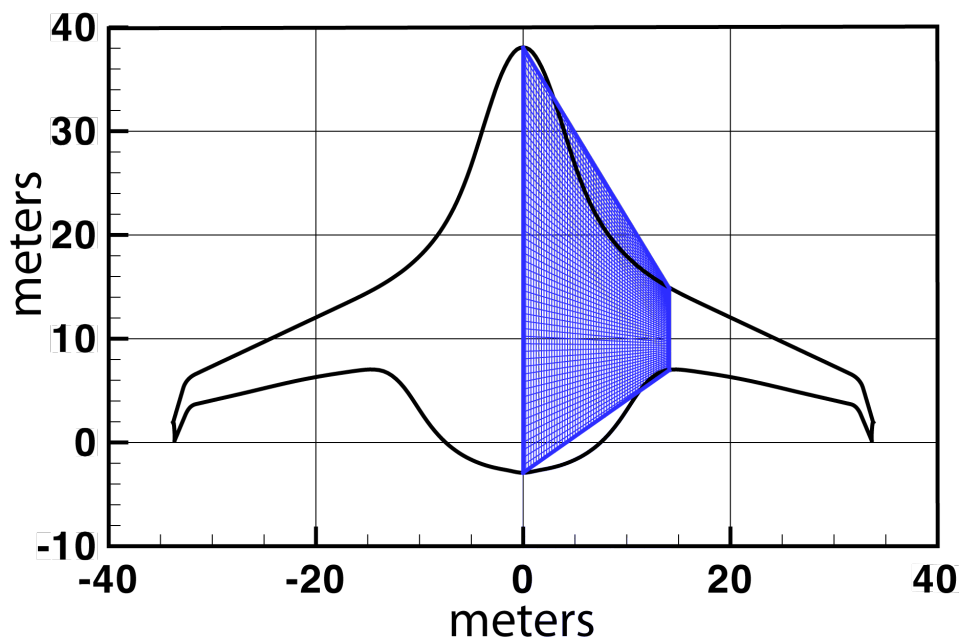


Figure 4. SAX 40 planform with shaded overlay defining the quadrilateral used to model the shielding body in the ANOPP WING module.

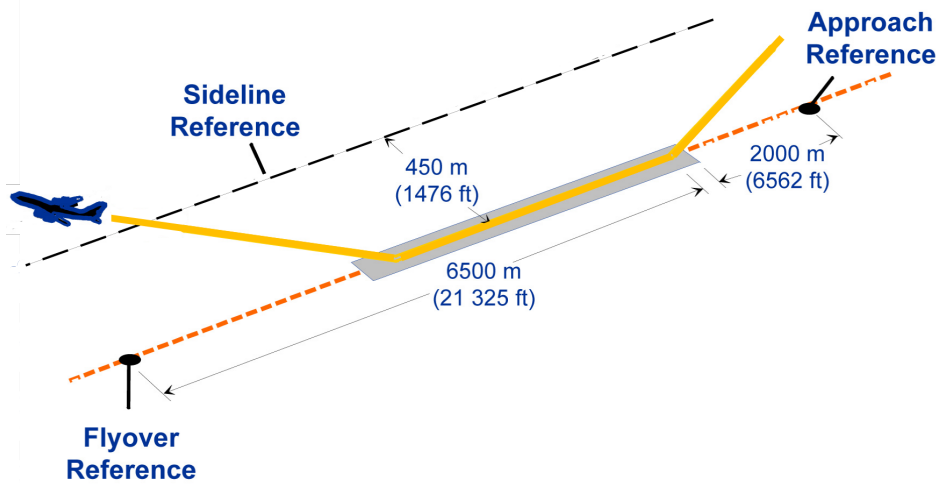


Figure 5. Noise certification measurement locations

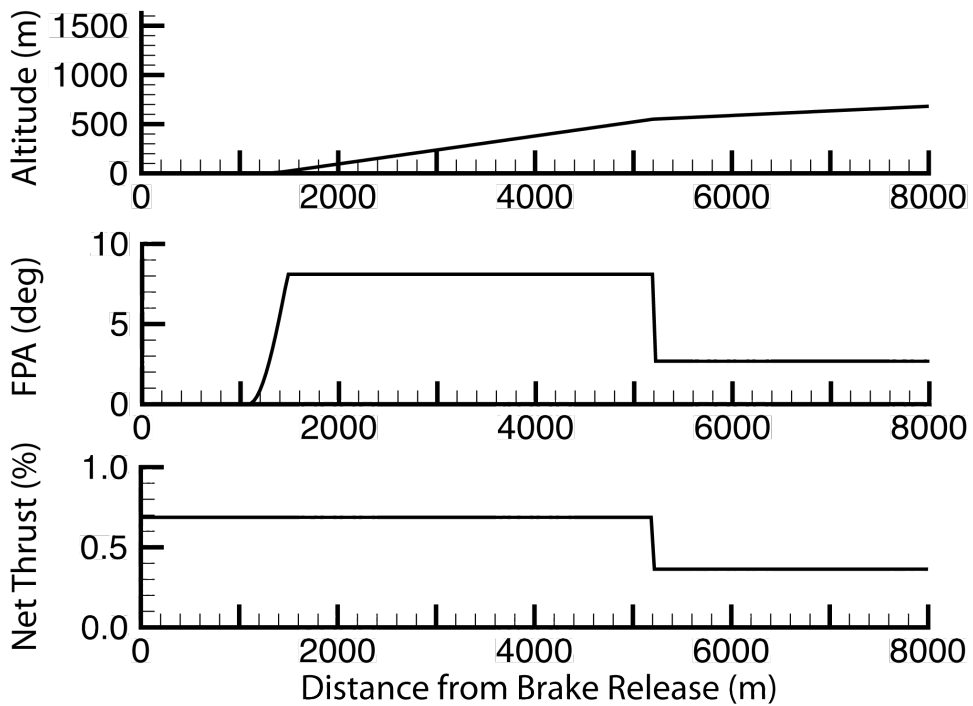


Figure 6. Takeoff flight trajectory variations for altitude, Flight Path Angle (FPA), and % of total net thrust.

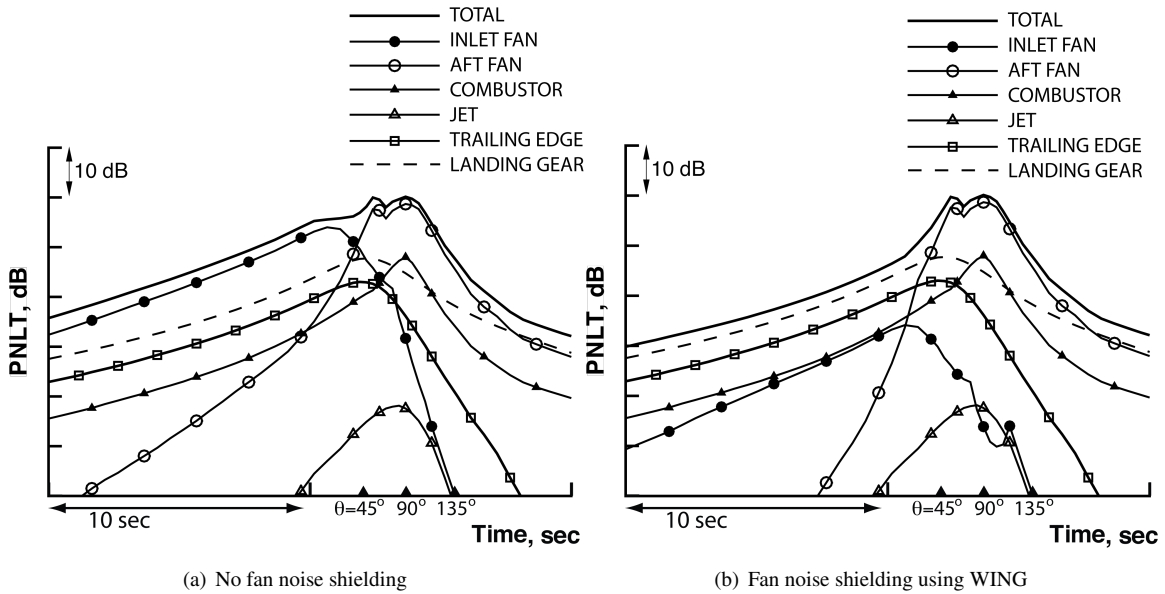


Figure 7. ANOPP predictions of PNLT for the approach reference location.

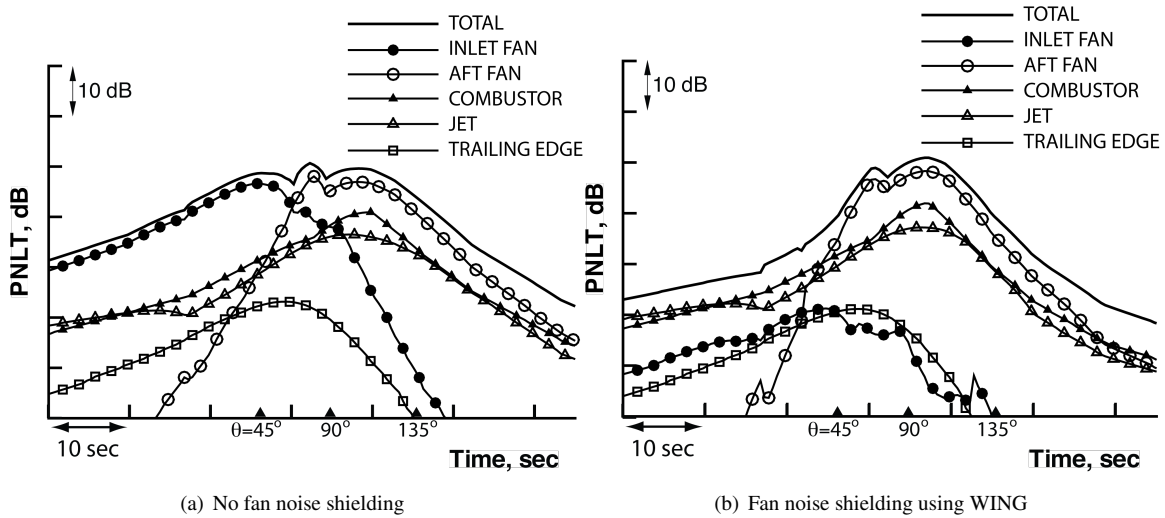
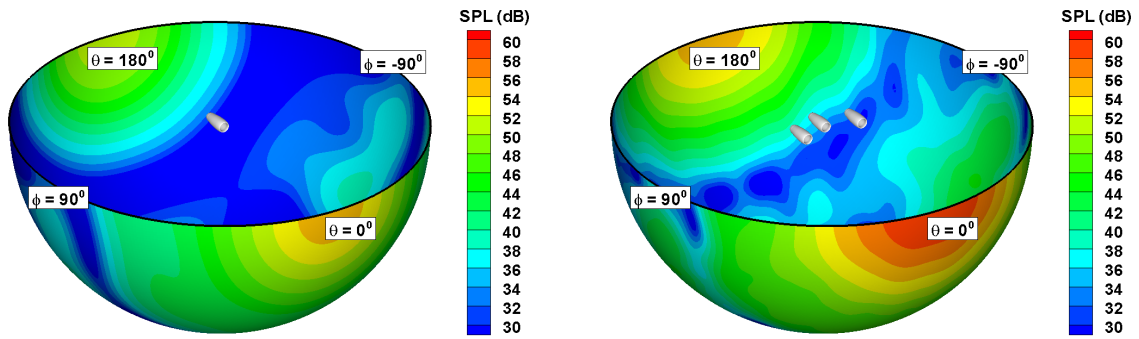
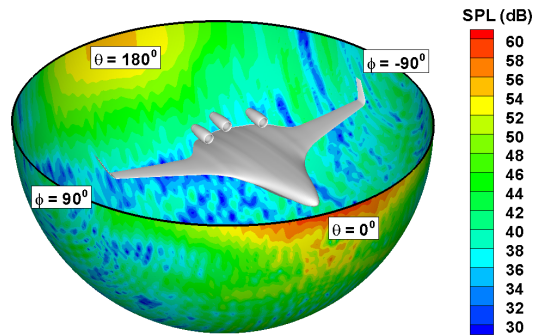


Figure 8. ANOPP predictions of PNLT for the flyover reference location.



(a) Center Nacelle Alone

(b) Three Nacelle Configuration



(c) Full Configuration

Figure 9. Predicted noise source semi-spheres showing the relative locations of the SAX 40 configuration and the RNM source semi-sphere. The source semi-sphere is centered on the fan face axial location (along the engine centerline) of the center nacelle. Absolute SPL levels are shown for a hypothetical fan source at a frequency of 200 Hz.

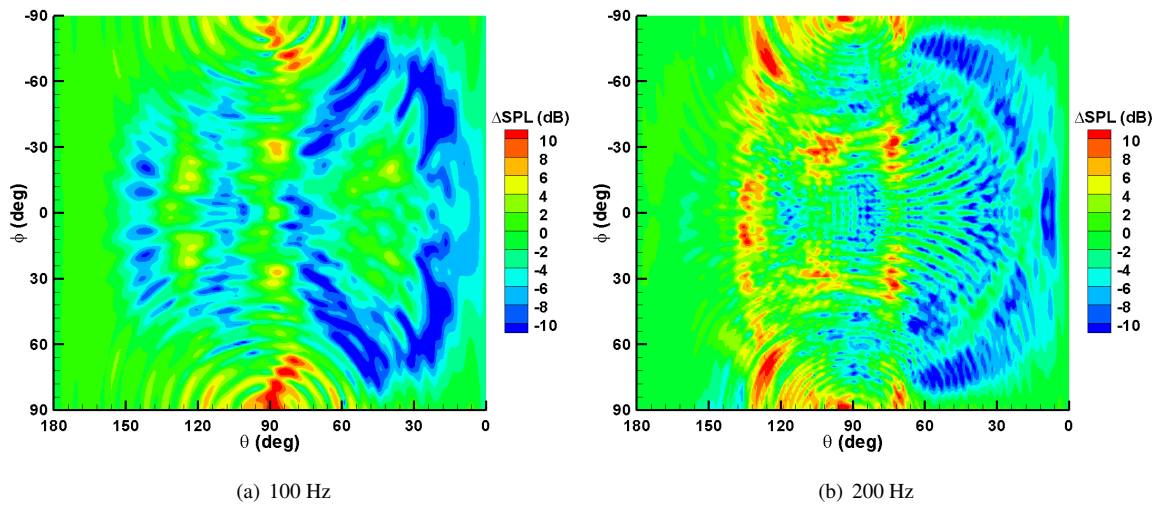


Figure 10. Δ SPL between shielded and unshielded three nacelle configuration on RNM source semi-sphere. Positive values indicate amplification, while negative values show suppression.

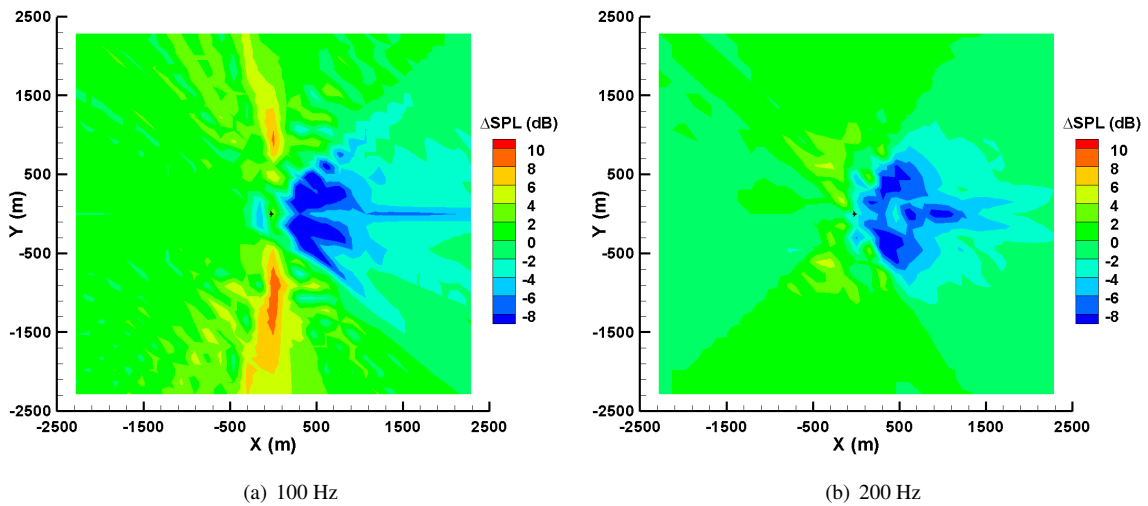
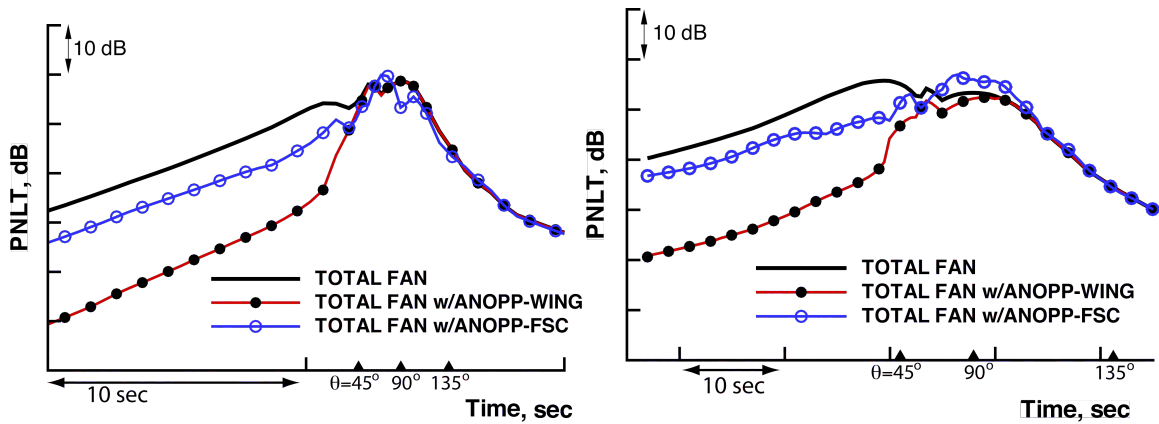
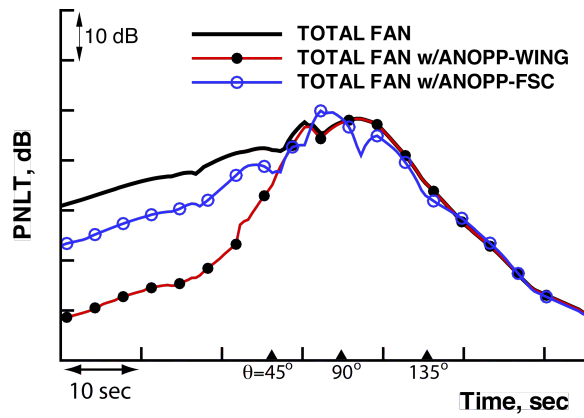


Figure 11. Footprints showing Δ SPL between shielded and unshielded three nacelle configuration. Positive values indicate amplification, while negative values show suppression.



(a) Approach reference location.

(b) Sideline reference location.



(c) Flyover reference location.

Figure 12. PNLT fan noise predictions at the three certification points. Note that the ANOPP-FSC predictions assume constant suppression function values from 400 Hz to 10 kHz due to current FSC frequency limitations for the full scale configuration.

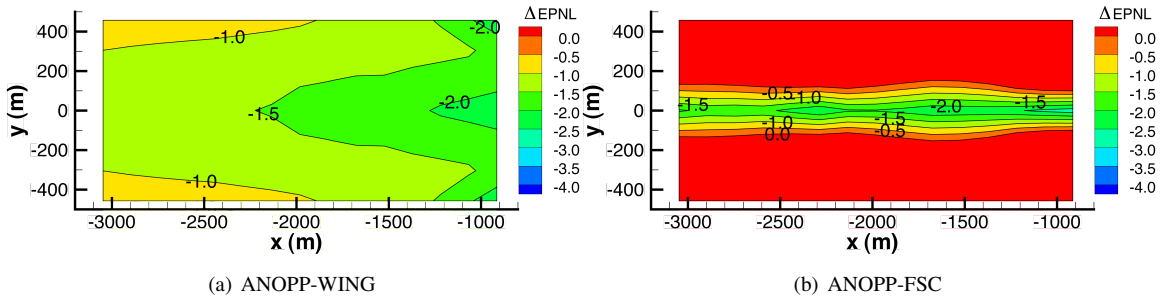


Figure 13. Comparison of predicted ΔEPNL contours for the approach flight condition. Note that the ANOPP-FSC predictions assume constant suppression function values from 400 Hz to 10 kHz due to current FSC frequency limitations for the full scale configuration.

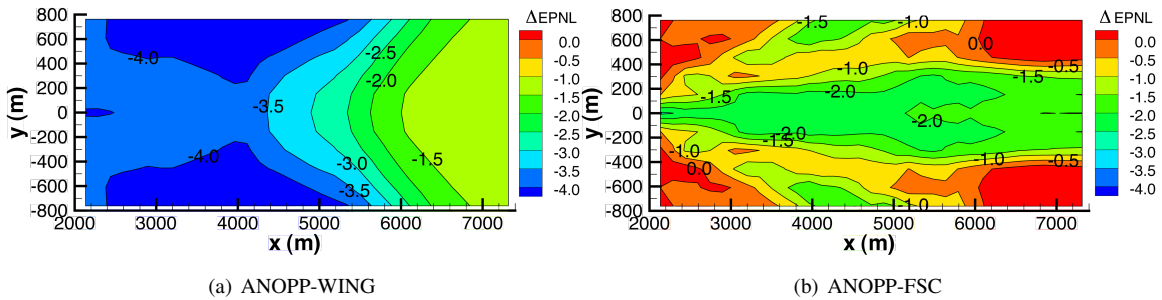


Figure 14. Comparison of predicted ΔEPNL contours for the takeoff flight condition. Note that the ANOPP-FSC predictions assume constant suppression function values from 400 Hz to 10 kHz due to current FSC frequency limitations for the full scale configuration.